Available online at www.sciencedirect.com

ScienceDirect

Procedia CIRP 87 (2020) 339–344

www.elsevier.com/locate/procedia

5th CIRP CSI 2020

On the surface integrity of additive manufactured and post-processed AlSi10Mg parts

Debajyoti Bhaduri[a,b,*], Pavel Penchev[b], Stefan Dimov[b], Khamis Essa[b], Luke N. Carter[c], Catalin I. Pruncu[b,d], Jun Jiang[d], Daniele Pullini[e]

[a] School of Engineering, Cardiff University, Queen's Buildings, The Parade, Cardiff, CF24 3AA, UK
[b] Department of Mechanical Engineering, School of Engineering, University of Birmingham, Edgbaston, Birmingham, B15 2TT, UK
[c] School of Metallurgy and Materials, University of Birmingham, Edgbaston, Birmingham, B15 2TT, UK
[d] Department of Mechanical Engineering, Imperial College London, South Kensington Campus, London, SW7 2AZ, UK
[e] C.R.F ScPA., Sede legale e amministrativa: Strada Torino, 50, 10043 Orbassano (TO), Italy

* Corresponding author. Tel.: +44 (0)29 2251 0922. *E-mail address:* BhaduriD@cardiff.ac.uk

Abstract

The research centres on the evaluation of surface integrity of AlSi10Mg parts produced via laser-based powder bed fusion (LPBF) process, followed by vibratory surface finishing. The alloy is chosen for its applications in lightweight components used in electronic packaging, automotive and aerospace sectors. Initial experiments involve optimisation of key LPBF process parameters by analysing the surface roughness and density data of the built parts. A Taguchi L_{18} orthogonal array is used for the optmisation trials with variations in the laser power (P), beam scanning speed (v), hatch spacing (H) and island size (I). Latter experimental phase deals with microhardness and microstructure assessment of heat treated LPBF specimens that are produced using the optimised LPBF parameters, i.e. P: 250 W, v: 1500 mm/s, H: 75 µm and I: 2 mm. Microhardnesses of the annealed samples reduce by ~12% with respect to the as-built parts and the values remain almost unchanged from the annealed state following solution treatment and ageing. The fish-scale like melt-pools observed on the unheat treated samples begin to fade off in the annealed specimens and completely disappear after solution treatment and ageing, with silicon particles dispersed all over the aluminium matrix. The final experimental phase involves vibratory surface finishing of the as-built LPBF parts using a vibrating ceramic media mixed with different acid and amine based liquid compounds for 1-6 hours, followed by vibrating in a maize based media for another 1-6 hours. The process aids in reducing the parts' roughness, S_a by ~35-70%, however the effect is more prominent when using the ceramic media.

Keywords: Laser-based powder bed fusion; aluminium; surface integrity

1. Introduction

Aluminium alloys are extensively used in the automotive, aerospace, electrical and electronic industry due to good castability, and a combination of their high strength and low density properties [1]. Recent trend of digital manufacturing, in line with the aims of Industry 4.0, has stimulated additive manufacturing (AM) of near net shape aluminium parts, with special interest in the AM of AlSi10Mg alloy via laser-based powder bed fusion (LPBF) process [2]. The choice of this Al alloy is motivated by the material's good weldability because of the near-eutectic composition of Al and Si, and improved hardenability properties as a result of the 0.3-0.5 wt.% Mg addition in the alloy that leads to precipitation hardening of aluminium by forming Mg_2Si during natural or artificial ageing heat treatments [3]. A comprehensive study has been undertaken on the LPBF, in particular, selective laser melting (SLM) of AlSi10Mg alloy over the past decade.

Early research on the SLM of aluminium alloy indicates that a high-power laser is needed to achieve fully dense Al

10.1016/j.procir.2020.02.093

parts in order to alleviate the high reflectivity, high thermal conductivity and low laser energy absorptivity of the material. Buchbinder et al. [4] showed that ~100% dense components can be produced only with laser power higher than 150 W. In a later study, Buchbinder et al. [5] reported that a right combination of laser power and beam scanning speed is required to fabricate dense components, for example a 300 W power with a scanning velocity of 500 mm/s or a 500 W power with a scan speed of 1200 mm/s can produce parts with nearly 100% density.

The majority of research on SLM of AlSi10Mg alloy has focussed on the process optimisation and the evaluation of microstructure and mechanical properties. Laser powers of 100-200 W have been typically employed together with scan speeds of 700-2000 mm/s and hatch spacings of 30-75 µm [6]. In relation to the mechanical properties, comparable/higher ultimate tensile strength (~396-399 MPa) as well as microhardness (~136-152HV) of the SLM AlSi10Mg parts were obtained upon T6 heat treatment with respect to that of the die cast samples (~300-365 MPa and ~95-133HV, respectively) [7], however at the expense of ~57-67% lower elongation at the break in the former specimens [6]. The heat treated samples generally exhibited ductile mode failures, characterised by typical dimple structures indicating micro-void coalescence, as opposed to the brittle failure of the as-built tensile bars due to the inherent SLM process-induced brittleness [8]. Heat treatment also influenced the fatigue performance of the SLM parts that was further affected by the build directions and imperfections such as porosity or shrinkage cavities [9,10].

The very fast cooling rate during SLM (~10^6-10^8 °C/s) renders a very fine cellular dendritic microstructure comprising fine distribution of diamond like cubic Si phase within the face centred cubic Al matrix [3]. Upon heat treatment, the density and the size of the Si particles grow larger leading to a composite-type microstructure consisting of soft α-Al regions reinforced with small Si particles [11].

Although the SLM process for AlSi10Mg alloy has been fairly optimised in terms of the finished parts' acceptable density, microstructure and mechanical properties, the as-built parts still suffer from high surface roughness (~4-15 µm), balling and stair-step effects [12,13] that could detriment the parts' fatigue life [9] and/or corrosion resistance [14]. A limited amount of study has been undertaken to improve the surface quality/roughness of the as-built SLM aluminium parts via laser polishing (LP) [15]. The technology aided in reducing R_a from 7.5-10.5 µm of the as-built surfaces to as low as 0.14-0.66 µm after LP [15]. However, the process could be expensive due to the requirement of a laser machine. Additionally, the technology yet has limitations in maintaining a uniform re-melting depth when polishing freeform surfaces over a larger processing area.

This paper initially reports optimisation of key SLM process parameters for AlSi10Mg parts, followed by microhardness and microstructure evaluation of the specimens before and after annealing and solution-ageing heat treatment. The capability of vibratory surface finishing method as an inexpensive alternative to laser polishing is then assessed on the as-built parts, using ceramic and maize based media. The rationale for using the vibratory polishing technique is further justified by its potential application to larger freeform components.

2. Experimental details

2.1. Selective laser melting of AlSi10Mg alloy parts

The SLM parts (10×10×10 mm^3) were produced using gas atomised AlSi10Mg alloy powders supplied by LPW Technology Ltd., with a particle size range of ~20-63 µm. Details of powder composition, morphology and flowability are furnished in [6]. All specimens were fabricated on a Concept Laser M2 Cusing® laser powder bed system, equipped with a Yb-fibre laser with 60 µm spot size, 150 µm laser track width and a vertical Z-increment of 30 µm in an Argon atmosphere with an oxygen-content <0.1%. An island scanning strategy was adopted to balance the residual stresses in the specimens, details given in [6]. After selective melting the islands, laser scans were carried out around the perimeter of the layer with the same process parameters to improve the surface finish. For each subsequent layer, these islands were translated by 1 mm in the X and Y-directions. Based on the literature [6], a Taguchi L_{18} orthogonal array comprising 18 trials and involving variations in laser power, P (100, 150, 200, 250, 300, and 350 W), scan speed, v (1000, 1500, and 2000 mm/s), hatch spacing, H (30, 75, and 120 µm) and island size, I (2, 5, and 8 mm) was undertaken to optimise the SLM process parameters in regard to the parts' surface roughness and relative density. The experimental array is shown in Table 1.

Table 1. Taguchi L_{18} orthogonal array.

Test No.	Laser power, P (W)	Scan speed, v (mm/s)	Hatch spacing, H (µm)	Island size, I (mm)
1	100	1000	30	2
2	100	1500	75	5
3	100	2000	120	8
4	150	1000	30	5
5	150	1500	75	8
6	150	2000	120	2
7	200	1000	75	2
8	200	1500	120	5
9	200	2000	30	8
10	250	1000	120	8
11	250	1500	30	2
12	250	2000	75	5
13	300	1000	75	8
14	300	1500	120	2
15	300	2000	30	5
16	350	1000	120	5
17	350	1500	30	8
18	350	2000	75	2

2.2. Heat treatment

Based on the optimisation trials nine additional SLM parts were built with a 250 W laser power, 1500 mm/s scan speed, 75 µm hatch spacing and 2 mm island size. Six of the nine specimens were subject to annealing/stress relieving at 300 °C

for 2 hours [16]. Three of the six annealed samples were solution heat treated at 510 °C for 6 hours, followed by water quenching and artificial ageing at 170 °C for another 4 hours [17]. The latter condition is hereinafter referred to as ST/A.

2.3. Vibratory surface finishing

Vibratory surface finishing (VSF) of the as-built SLM cubes (without any heat treatment) were carried out using a Sharmic AV75 tumbling machine operating at 50 Hz vibration frequency. Details of the commercial polishing media and the corresponding VSF time durations before measuring the surface roughness are presented in Table 2.

Table 2. Details of the VSF media used and the corresponding time durations.

Specimens	Test conditions	Media used	Surface roughness measured after VSF for
1A) Set 1 as-built SLM cubes	CAc	10 mm triangular ceramic media (mixture of aluminium oxide, clays, quartz and kaolin), mixed with NORCHEM 80 liquid compound (mixture of citric acid monohydrate, alcohols, diethanolamine, amides and lauric acid) [18]	1, 2, 3, 4 and 6 h
1B) Specimens undergone CAc for 6 h	Maizeorb	Natural corn-cob in granules	1, 2, 3, 4 and 6 h
2A) Set 2 as-built SLM cubes	CAm	10 mm triangular ceramic media, mixed with SX-1L liquid compound (mixture of diethanolamine, amides, lauric acid and sodium lauroyl sarcosinate) [18]	1, 2, 3, 4 and 6 h
2B) Specimens undergone CAm for 6 h	Maizeorb	Natural corn-cob in granules	1, 2, 3, 4 and 6 h

2.4 Analysis equipment used

The 3D surface parameters S_a and S_z of the as-built and VSF SLM cubes was measured with an Alicona G5 InfiniteFocus microscope, on their top face as well as four side faces over 2.26 × 2.26 mm^2, using a 20X objective. For the side faces, an average of four roughness data measured on four side faces of each cube was considered. Minitab 17 software was used for statistical analysis. The relative density of the SLM parts were determined via Archimedes principle by weighing the samples in air and ethanol.

The as-built and heat treated parts were wire-cut along longitudinal and transverse SLM build directions (LBD and TBD planes, respectively), followed by mounting and mechanical polishing. Vickers microhardness measurements were carried out on LBD and TBD planes using a 100 g load and indent time of 15 s. Five measurements were recorded on both planes, and the average was calculated.

The as-built and the heat treated samples were immersion etched in Keller's reagent (2 mL hydrofluoric acid, 3 mL hydrochloric acid, 5 mL nitric acid and 190 mL deionised water) for 45 s and were observed under a Leica DMLM optical microscope for microstructure analysis. The specimens were further characterised for grain orientation using a Hitachi 3400 SEM based Bruker e-flash electron backscatter diffraction (EBSD) detector at 20kV acceleration voltage, 10 µA current density and 1 µm step size with the images further post-processed using MTEX software.

3. Results and discussion

3.1. Optimisation of SLM process parameters

The main effects of the key SLM process parameters on the as-built parts' top and side face roughness S_a and relative density are shown in Fig. 1(a), 1(b) and 1(c) respectively. Laser power (P) has the greatest influence (statistically significant) on both top and side face S_a with percentage contribution ratios (PCRs) 91.2 and 55.2, respectively.

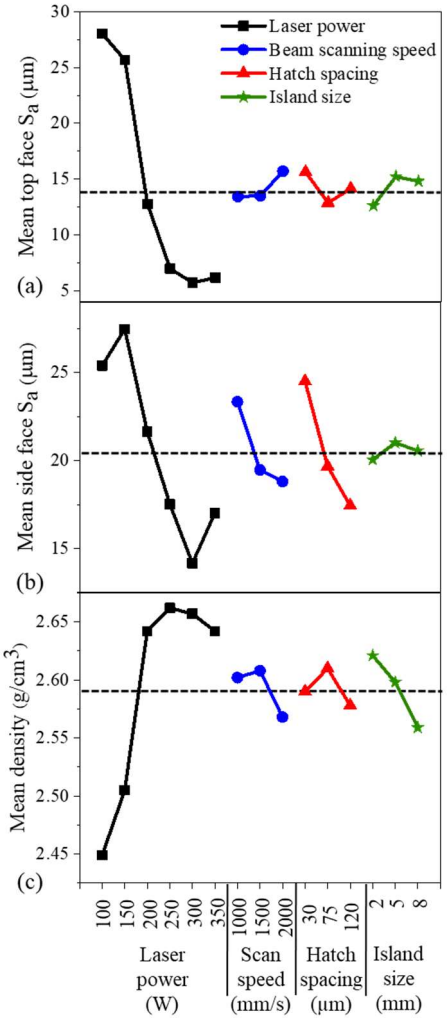

Fig. 1. Main effects of the SLM process parameters on (a) top face roughness; (b) side face roughness; and (c) density of the as-built parts.

All other SLM parameters, viz. beam scanning speed (v), hatch spacing (H) and island size (I) have marginal contributions on top face S_a, whereas the PCRs of v and H for side face S_a are 9.8 and 21.3 respectively. The trend in the surface roughness data has clear reflection on the topography images (Fig. 2). Insufficient melting and numerous balling and satellite formation are observed on the top and side faces

when processed using 100 W laser power (Test 1). Increasing the laser power to 250-300 W assists in maintaining the melt-pool and thus evidently improves the surface morphology, with minimal balling and fewer tiny satellites visible on the top and side faces. Representative images taken after Test 11 and Test 15 are shown in Fig. 2(b) and 2(d), respectively. The minimum top and side face S_a obtained are 3.9 and 13.6 µm.

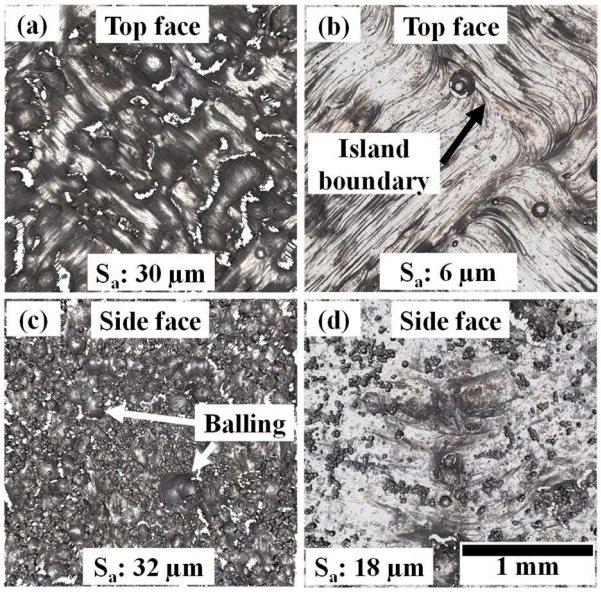

Fig. 2. Surface topographies of as-built SLM parts, taken on top faces after (a) Test 1; (b) Test 15 and on side faces following (C) Test 1; (d) Test 11.

In regard to the density of the SLM parts, power (P) again has the maximum influence with a 79.2 PCR. As the primary concern for the SLM process is to build fully dense components the optimsed SLM parameters selected are mainly based on the density results. A 250 W laser power together with a scan speed of 1500 mm/s, hatch spacing of 75 µm and island size of 2 mm is utilised for building the specimens for heat treatment (for microhardness and microstructure analysis) and VSF trials. It is also envisaged that these parametric combination would render comparable surface roughness to that recorded after Test 11.

3.2. Microhardness and microstructure analysis

Comparable microhardness values, in the range of ~97-99$HV_{0.1}$, are measured on the LBD and TBD planes of the as-built SLM samples, see Fig. 3. Microhardness reduces by ~12% upon annealing (varies between ~83-88$HV_{0.1}$ on both LBD and TBD planes) and the data remain almost unchanged following ST/A (~83-84$HV_{0.1}$). The values are somewhat lower than that reported by Rosenthal and Stern [19], which are 125±5HV for the as-built parts and 107±5HV after stress relief. A much lower microhardness (~88HV) is however measured by Maamoun et al. [2] when SLM with a ~64 J/mm^3 laser energy density, whereas the present samples are prepared with an energy density of 74 J/mm^3. They also reported a hardness of ~98HV on the LBD plane when using a laser power of 250 W which is comparable with the current study. On the TBD plane however they measured ~15% higher microhardness (~116HV) when using a 250 W power.

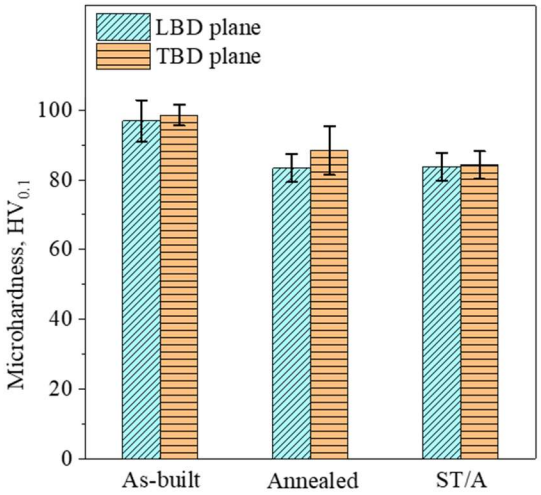

Fig. 3. Microhardness data of the SLM parts before and after heat treatment.

The cross-sectional microstructure along the build direction of the unheat treated specimens exhibits typical fish-scale like structures of ~100-200 µm size, in agreement with the Gaussian profile of the laser beam, see Fig. 4(a). Similar structures are also reported by several researchers [20]. Conversely, laser scan tracks are visible on the transverse build plane (Fig. 4(b)). An enlarged image in Fig. 4(c) reveals fine cellular structures inside the melt-pools in contrast to the coarser structures towards the melt-pool boundaries. The observation is in accordance with the faster cooling and solidification rate towards the melt-pool centre. Upon annealing, the melt-pool boundaries initiate to fade off and after ST/A melt-pools completely disappear leaving globular Si particles dispersed all over the α-Al matrix, as shown in Fig. 4(d). This occurs due to the coarsening and precipitation of Si upon heat treatment from a supersaturated state [9].

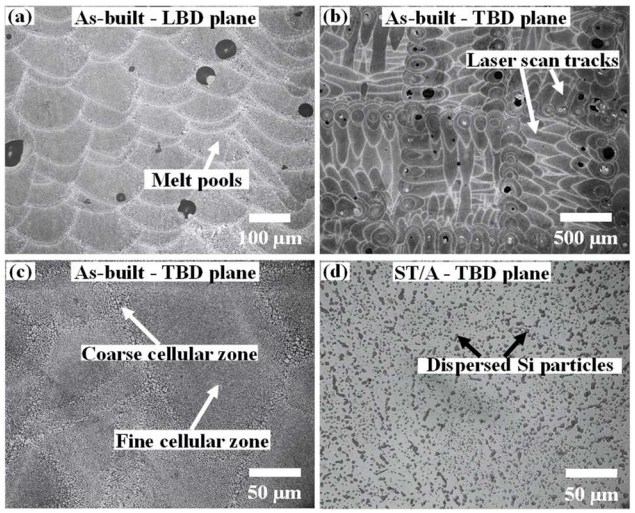

Fig. 4. Microstructure of SLM sections (a) as-built, taken on LBD plane; (b) as-built, viewed on TBD plane; (c) magnified view of (b); (d) after ST/A, seen on TBD plane.

The EBSD inverse pole figure in Fig. 5(a) shows elongated grains along the build direction, grown towards the centre of the melt-pools. Small nearly equiaxed grains are visible at the vicinity of the melt-pool boundaries, shown by white dashed lines. Similar observations are also made by Liu et al. [21].

Grain size gradually decreases following annealing (Fig. 5(b)) and ST/A (Fig. 5(c)). Greater homogenous grain structure coupled with the formation of smaller equiaxed grains takes place upon heat treatment. The corresponding geometrically necessary dislocation (GND) density maps also reveal that GNDs are not evenly distributed within the as-built and annealed grains, indicated by the local regions of high GND density (bright regions in Fig. 5(a) and 5(b)). The dislocation density however reduces after solution treatment and ageing.

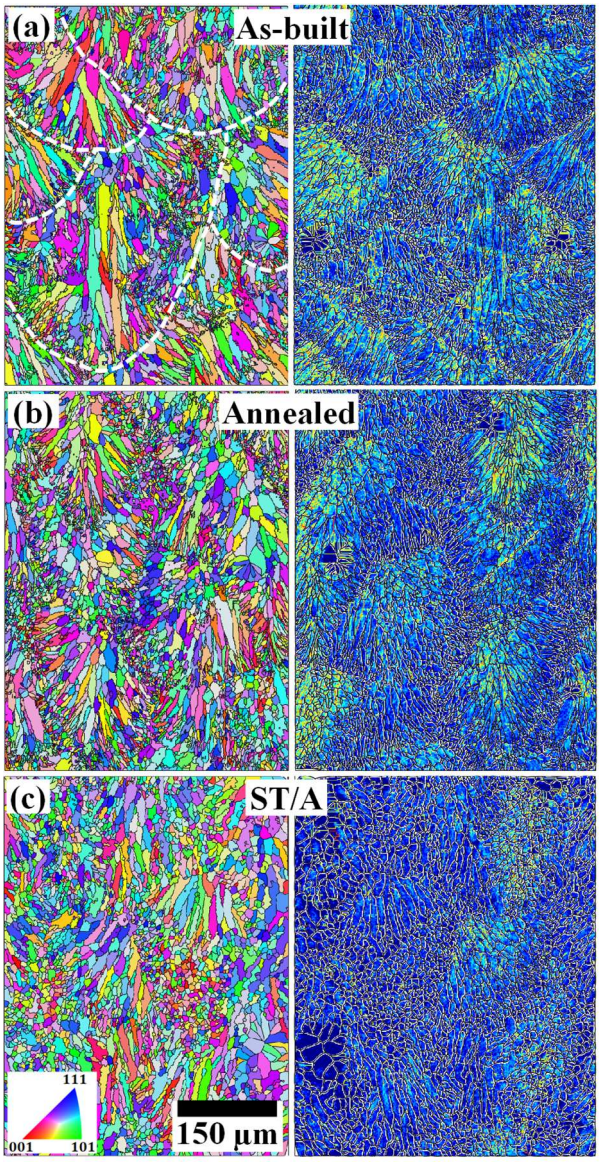

Fig. 5. EBSD inverse pole figures and the corresponding GND density maps for (a) as-built; (b) annealed and (c) ST/A SLM parts, seen on LBD planes.

3.3. Vibratory surface finishing

Vibratory surface finishing using the ceramic and acid based media (CAc condition) aids in reducing the top face roughness S_a and S_z by up to ~70% and ~83% respectively, however the effect is more prominent within 2-3 hours of surface treatment. Beyond this, roughness somewhat increases, possibly due to over erosion of surfaces by the sharp ceramic triangles, see Fig. 6. Use of a maize based media for fine surface treatment however does not significantly improve the surface quality over a processing duration of 6 h. VSF using the ceramic and amine based media (CAm condition) also exhibits similar situations as observed with the CAc media. Both S_a and S_z decrease by ~63-64% and ~75-81% respectively from the parent cubes' roughness, within 1-2 h of VSF. Use of maizeorb following CAm sometimes even aggravates the roughness values.

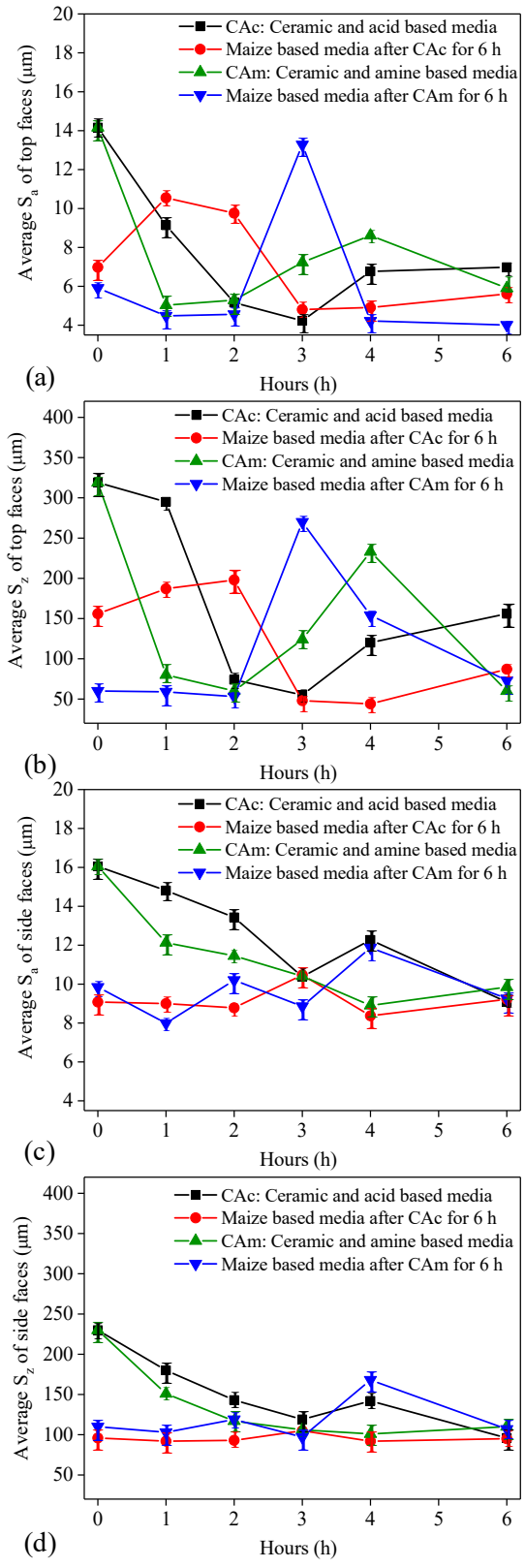

Fig. 6. Roughness (a) S_a and (b) S_z of top faces; (c) S_a and (d) S_z of side faces of as-built SLM cubes.

Similar to the top face, the S_a and S_z of side faces also drop by up to ~35% and ~48% within 3 h of VSF under the CAc condition. Comparably, use of the ceramic and amine based media assists in reducing S_a and S_z by up to ~45% and ~56% respectively after processing the samples for 4 h. However, the roughness values do not considerably alter following VSF with fine maizeorb based media.

The surface morphology images of the as-built and VSF top faces clearly show the evidence of the removal of larger surface particles, such as balling or partially melted powders (Fig. 7(a), 7(b)). Similarly, minimal presence of tiny satellites is apparent on the VSF side face, only a few eroded larger particles are visible following CAc for 3 h, see Fig. 7(c), 7(d).

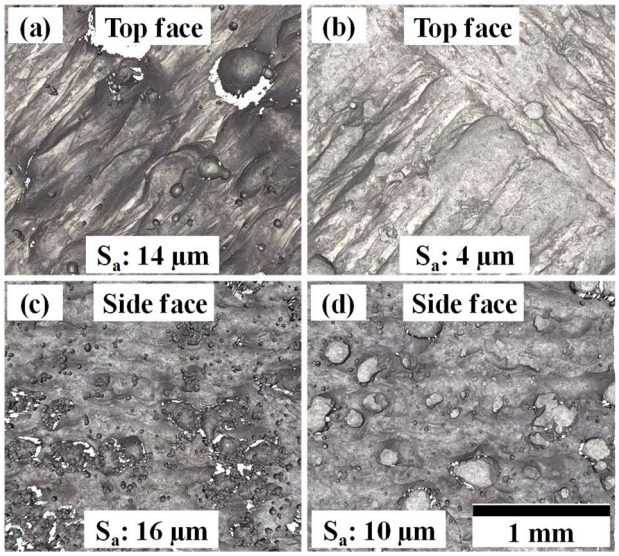

Fig. 7. Top surface of (a) as-built and (b) after VSF with maize for 6 h after CAc for 6 h; Side face of (c) as-built and (d) after VSF under CAc for 3 h.

4. Conclusions

Following optimisation of SLM process parameters for AlSi10Mg alloy this research investigates microhardness and microstructure alteration upon annealing, and solution treating and ageing. Additionally, the study proposes an inexpensive post-processing/polishing technique for large freeform AM parts using vibratory surface finishing method. Based on the VSF results, it is inferred that a rough finishing routine using larger ceramic particle-based media would minimise/remove bigger surface particles within 2-3 h of treatment via abrasion/mechanical erosion. The minimum S_a obtained on the top and side faces are ~4 and 8 µm respectively. Beyond that, the surface quality might deteriorate due to further abrasion with the ceramic particles. Use of smaller grains (e.g. maizeorb) for fine surface finishing may not add extra benefit to the surface quality as the particles would possibly be too tiny to erode large surface particles that effectively contribute to the roughness in greater proportion.

Acknowledgements

The research is supported by the European Union's Horizon 2020 research and innovation programme under the grant agreement No 723826 (MAESTRO).

References

[1] Wu J, Wang XQ, Wang W, Attallah MM, Loretto MH. Microstructure and strength of selectively laser melted AlSi10Mg. Acta Mater 2016;117:311-320.
[2] Maamoun AH, Xue YF, Elbestawi MA, Veldhuis SC. The effect of selective laser melting process parameters on the microstructure and mechanical properties of Al6061 and AlSi10Mg alloys. Materials 2019;12,12.
[3] Thijs L, Kempen K, Kruth J-P, Humbeeck JV. Fine-structured aluminium products with controllable texture by selective laser melting of pre-alloyed AlSi10Mg powder. Acta Mater 2013;61:1809-1819.
[4] Buchbinder D, Meiners W, Wissenbach K, Müller-Lohmeier K, Brandl E. Rapid manufacturing of aluminium parts for serial production via selective laser melting (SLM). Proc 11th Int Conf on Aluminium Alloys, Aachen, Germany. 2008:2394-2400.
[5] Buchbinder D, Schleifenbaum H, Heidrich S, Meiners W, Bültmann J. High power selective laser melting (HP SLM) of aluminum parts. Phys Procedia 2011;12:271-278.
[6] Read N, Wang W, Essa K, Attallah MM. Selective laser melting of AlSi10Mg alloy: Process optimisation and mechanical properties development. Mater Des 2015;65:417-424.
[7] Kempen K, Thijs L, Humbeeck JV, Kruth J-P. Processing AlSi10Mg by selective laser melting: parameter optimisation and material characterisation. Mater Sci Technol 2015;31/8:917-923.
[8] Aboulkhair NT, Maskery I, Tuck C, Ashcroft I, Everitt NM. The microstructure and mechanical properties of selectively laser melted AlSi10Mg: The effect of a conventional T6-like heat treatment. Mater Sci Eng A 2016;667:139-146.
[9] Brandl E, Heckenberger U, Holzinger V, Buchbinder D. Additive manufactured AlSi10Mg samples using Selective Laser Melting (SLM): Microstructure, high cycle fatigue, and fracture behavior. Mater Des 2012;34:159-169.
[10] Uzan NE, Shneck R, Yeheskel O, Frage N. Fatigue of AlSi10Mg specimens fabricated by additive manufacturing selective laser melting (AM-SLM). Mater Sci Eng A 2017;704:229-237.
[11] Prashanth KG, Scudino S, Klauss HJ, Surreddi KB, Löber L, Wang Z, Chaubey AK, Kühn U, Eckert J. Microstructure and mechanical properties of Al-12Si produced by selective laser melting: Effect of heat treatment. Mater Sci Eng A 2014;590:153-160.
[12] Wang L-z, Wang S, Wu J-j. Experimental investigation on densification behavior and surface roughness of AlSi10Mg powders produced by selective laser melting. Optics Laser Technol 2017;96:88-96.
[13] Maamoun AH, Xue YF, Elbestawi MA, Veldhuis SC. Effect of selective laser melting process parameters on the quality of Al alloy parts: Powder characterization, density, surface roughness, and dimensional accuracy. Materials 2018;11:2343.
[14] Leon A, Aghion E. Effect of surface roughness on corrosion fatigue performance of AlSi10Mg alloy produced by Selective Laser Melting (SLM). Mater Charac 2017;131:188-194.
[15] Hofele M, Schanz J, Burzic B, Lutz S, Merkel M, Riegel H. Laser based post processing of additive manufactured metal parts. Lasers in Manuf LIM 2017 Conf, Munich, Germany. 2017.
[16] Takata N, Kodaira H, Sekizawa K, Suzuki A, Kobashi M (2017) Change in microstructure of selectively laser melted AlSi10Mg alloy with heat treatments. Materials Science & Engineering A 704:218-228.
[17] Mertens A, Dedry O, Reuter D, Rigo O, Lecomte-Beckers J. Thermal treatments of AlSi10Mg processed by laser beam melting. Proc 26th Int Solid Freeform Fabrication Sympo 2015;1007-1016.
[18] Materials safety data sheet, Sharmic Engineering Ltd., UK.
[19] Rosenthal I, Stern A. Heat treatment investigation of the AlSi10Mg alloy Produced by selective laser melting (SLM): Microstructure and hardness. Welding Equip Technol 2017;27:7-11.
[20] Zhang C, Zhu H, Liao H, Cheng Y, Hu Z, Zeng X. Effect of heat treatments on fatigue property of selective laser melting AlSi10Mg. Int J Factigue 2018;116:513-522.
[21] Liu X, Zhao C, Zhou X, Shen Z, Liu W. Microstructure of selective laser melted AlSi10Mg alloy. Mater Des 2019;168:107677.